

Supplementary Information
CoolWalks for active mobility in urban street networks

Henrik Wolf^{a,b}, Ane Rahbek Vierø^a, and Michael Szell^{a,c,d}

^a *NEtworks, Data and Society (NERDS), Computer Science Department, IT University of Copenhagen, Copenhagen, 2300, Denmark*

^b *Chair for Network Dynamics, Institute for Theoretical Physics and Center for Advancing Electronics Dresden (cfaed), Technical University of Dresden, Dresden, 01307, Germany*

^c *ISI Foundation, Turin, 10126, Italy*

^d *Complexity Science Hub Vienna, Vienna, 1080, Austria*

This is the supplementary information for the manuscript containing supplementary notes and figures.

Supplementary Note 1: Data acquisition

Street networks

We used OpenStreetMaps as the source for the studied street networks of Manhattan, Barcelona and Valencia, which can be conveniently accessed via the Overpass query language. Below are the query strings we used for downloading the pedestrian and cycling networks, respectively. Note the use of [bbox:{bbox}] as a spatial filter, used here to enable copying into overpass turbo. In the real application, this was replaced by the bounding box of the study area.

```
[out:json][timeout:180][bbox:{bbox}];  
way["highway"]["area"!~"yes"]  
  ["highway"!~"cycleway|motor|proposed"]  
  ["highway"!~"construction|abandoned|platform|raceway"]  
  ["foot"!~"no"]  
  ["access"!~"private"]  
  ["service"!~"private"];  
(._.;>);  
out count;  
out ;
```

Listing 1: Overpass query for pedestrian networks.

```
[out:json][timeout:180][bbox:{bbox}];  
way["highway"]  
  ["area"!~"yes"]  
  ["highway"!~"footway|steps|corridor|elevator|escalator"]  
  ["highway"!~"motor|proposed|construction"]  
  ["highway"!~"abandoned|platform|raceway"]  
  ["bicycle"!~"no"]  
  ["access"!~"private"]  
  ["service"!~"private"];  
(._.;>);  
out count;  
out ;
```

Listing 2: Overpass query for cycling networks.

When loading the networks from the resulting files, we ignore possible one-way streets by adding all non-existent reverse edges to the street graph.

Buildings

New York City

The building data for Manhattan was provided by the New York City Office of Technology and Innovation [1]. It includes the footprints of New York City buildings as well as the height of their roofs above the ground.

Spain

The building data for Barcelona as well as Valencia was provided by the General Directorate for Cadastre of Spain [2]. The available datasets contain the building footprints for the buildings in the respective region together with additional polygons representing segments of the buildings which can be used to map variations in height across the associated building. Neither the footprints of buildings nor their segments come with a directly accessible height value, and only the segments have a value for the number of floors available. We therefore assume a constant height of 4 m per floor.

It would, in theory, be possible to use the segments transformed in this way directly as the input for our analysis. However, the large amount of segments compared to the number of buildings would result in increased computational requirements. As such, we approximate the height of each building by the area-weighted average of the heights of each of its segments.

Supplementary Note 2: Analytical derivations

CoolWalkability on grids - general form

Starting from main text Eq. 6, we derive the analytical expression for the CoolWalkability on a city with a perfect, infinite grid-like street network and buildings of constant height and shape.

When writing main text Eq. 1 for $l_{ij}^{\diamond} = 0$

$$\lambda_{ij} = l_{ij}^{\bullet} = l_{ij} \quad (\text{SI1})$$

and $l_{ij}^{\bullet} = 0$

$$\lambda_{ij} = \alpha \cdot l_{ij}^{\diamond} = \alpha \cdot l_{ij} \quad (\text{SI2})$$

we see that for these extreme cases, the felt lengths only differ by the constant factor α . As such, paths which minimize $\Lambda_{i \rightarrow j}^{\alpha}(0)$ minimize $\Lambda_{i \rightarrow j}^{\alpha}(1)$ as well. More specifically, we get $\Lambda_{i \rightarrow j}^{\alpha,*}(0) = \alpha \cdot \Lambda_{i \rightarrow j}^{1,*}$ and $\Lambda_{i \rightarrow j}^{\alpha,*}(1) = \Lambda_{i \rightarrow j}^{1,*}$. Plugging these results into main text Eq. 6 yields

$$C^{\alpha}(t) = \frac{\sum (\Lambda_{i \rightarrow j}^{\alpha,*}(0) - \Lambda_{i \rightarrow j}^{\alpha,*}(\{S_{ab}\}))}{\sum (\Lambda_{i \rightarrow j}^{\alpha,*}(0) - \Lambda_{i \rightarrow j}^{\alpha,*}(1))} = \frac{\sum (\alpha \cdot \Lambda_{i \rightarrow j}^{1,*} - \Lambda_{i \rightarrow j}^{\alpha,*}(\{S_{ab}\}))}{\sum (\alpha \cdot \Lambda_{i \rightarrow j}^{1,*} - \Lambda_{i \rightarrow j}^{1,*})} = \frac{\sum (\alpha \cdot \Lambda_{i \rightarrow j}^{1,*} - \Lambda_{i \rightarrow j}^{\alpha,*}(\{S_{ab}\}))}{(\alpha - 1) \cdot \sum \Lambda_{i \rightarrow j}^{1,*}} \quad (\text{SI3})$$

where for better legibility, we omitted the summation indices over all reachable destinations. Expanding the sum in the numerator results in

$$C^{\alpha}(t) = \frac{1}{\alpha - 1} \left[\alpha - \frac{\sum_{i \in V_{\text{src}}, j \in V_{\text{dst}}(i)} \Lambda_{i \rightarrow j}^{\alpha,*}(\{S_{ab}\})}{\sum_{i \in V_{\text{src}}, j \in V_{\text{dst}}(i)} \Lambda_{i \rightarrow j}^{1,*}} \right] \quad (\text{SI4})$$

which is still correct for general street networks. Each vertex in a grid is identified by two coordinates (x, y) pointing at a column and row, relative to an arbitrarily chosen origin $(0, 0)$. A path is then denoted by $(x_1, y_1) \rightarrow (x_2, y_2)$. Using the translational invariance of the infinite grid, any such path is equivalent to the same path shifted to the origin,

$$(x_1, y_1) \rightarrow (x_2, y_2) \equiv (0, 0) \rightarrow (x_2 - x_1, y_2 - y_1). \quad (\text{SI5})$$

As such, the sums over index i in equation SI4 only result in a factor $|V_{\text{src}}|$ which cancels out. For only the expression in question we get

$$\frac{\sum_{i \in V_{\text{src}}, j \in V_{\text{dst}}(i)} \Lambda_{i \rightarrow j}^{\alpha,*}(\{S_{ab}\})}{\sum_{i \in V_{\text{src}}, j \in V_{\text{dst}}(i)} \Lambda_{i \rightarrow j}^{1,*}} = \frac{\sum_{(x,y) \in V_{\text{dst}}((0,0))} \Lambda_{(0,0) \rightarrow (x,y)}^{\alpha,*}(\{S_{ab}\})}{\sum_{(x,y) \in V_{\text{dst}}((0,0))} \Lambda_{(0,0) \rightarrow (x,y)}^{1,*}} \quad (\text{SI6})$$

On a rectangular grid with two types of edges a and b the length of any shortest path is given by

$$\Lambda_{(x_1, y_1) \rightarrow (x_2, y_2)}^{\alpha,*} = |x_2 - x_1| \cdot \lambda_a + |y_2 - y_1| \cdot \lambda_b = |\Delta x| \cdot \lambda_a + |\Delta y| \cdot \lambda_b \quad (\text{SI7})$$

which, in Eq. SI6 gives

$$\frac{\sum_{(x,y) \in V_{\text{dst}}((0,0))} \Lambda_{(0,0) \rightarrow (x,y)}^{\alpha,*}(\{S_{ab}\})}{\sum_{(x,y) \in V_{\text{dst}}((0,0))} \Lambda_{(0,0) \rightarrow (x,y)}^{1,*}} = \frac{\sum_{(\Delta x, \Delta y) \in V_{\text{dst}}} |\Delta x| \cdot \lambda_a + |\Delta y| \cdot \lambda_b}{\sum_{(\Delta x, \Delta y) \in V_{\text{dst}}} |\Delta x| \cdot l_a + |\Delta y| \cdot l_b} \quad (\text{SI8})$$

with

$$n = \sum_{(\Delta x, \Delta y) \in V_{\text{dst}}} |\Delta x| \quad m = \sum_{(\Delta x, \Delta y) \in V_{\text{dst}}} |\Delta y| \quad (\text{SI9})$$

we get the CoolWalkability SI4 on the grid as

$$\begin{aligned} C^\alpha(t) &= \frac{1}{\alpha - 1} \left[\alpha - \frac{n \cdot \lambda_a + m \cdot \lambda_b}{n \cdot l_a + m \cdot l_b} \right] \\ &= \frac{1}{\alpha - 1} \left[\alpha - \frac{n \cdot (\alpha \cdot l_a^* + l_a^\bullet) + m \cdot (\alpha \cdot l_b^* + l_b^\bullet)}{n \cdot l_a + m \cdot l_b} \right] \\ &= \frac{1}{\alpha - 1} \left[\alpha - \frac{n \cdot (\alpha [l_a - l_a^\bullet] + l_a^\bullet) + m \cdot (\alpha [l_b - l_b^\bullet] + l_b^\bullet)}{n \cdot l_a + m \cdot l_b} \right] \\ &= \frac{1}{\alpha - 1} \left[\alpha - \frac{\alpha [n l_a + m l_b] + (1 - \alpha) [n l_a^\bullet + m l_b^\bullet]}{n \cdot l_a + m \cdot l_b} \right] \end{aligned} \quad (\text{SI10})$$

Simplifying this equation gives the shape of the resulting main text Eq. 7:

$$C^\alpha = \frac{1}{\alpha - 1} \left[\alpha - \alpha - (1 - \alpha) \frac{n l_a^\bullet + m l_b^\bullet}{n l_a + m l_b} \right] = \frac{n l_a^\bullet + m l_b^\bullet}{n l_a + m l_b} \quad (\text{SI11})$$

CoolWalkability in the large trip-length limit

To solve the equation

$$n = \sum_{(\Delta x, \Delta y) \in V_{\text{dst}}} |\Delta x| \quad (\text{SI12})$$

we need to describe the set V_{dst} , which contains all the vertices of the grid reachable within r in Manhattan distance from the center. Geometrically, it contains all grid-point within a square with edge length of $\sqrt{2}r$ centered around $(0, 0)$ with the diagonals aligned with the directions of the grid. The maximal number of jumps in x direction is therefore

$$\Delta x_{\max} = \left\lfloor \frac{r}{l_a} \right\rfloor \quad (\text{SI13})$$

given a number of jumps Δx in x direction, we find the maximal number of jumps possible in y direction as

$$\Delta y_{\max}(\Delta x) = \left\lfloor \frac{r - l_a |\Delta x|}{l_b} \right\rfloor \quad (\text{SI14})$$

using the symmetry of the grid we express equation SI12 as a double sum with dependent limits

$$n = \sum_{(\Delta x, \Delta y) \in V_{\text{dst}}} |\Delta x| = \sum_{\substack{\Delta x = \\ -\Delta x_{\max}}}^{\Delta x_{\max}} \left(\sum_{\substack{\Delta y = \\ -\Delta y_{\max}(\Delta x)}}^{\Delta y_{\max}(\Delta x)} |\Delta x| \right) \quad (\text{SI15})$$

where we directly evaluate the inner sum as

$$n = \sum_{\substack{\Delta x = \\ -\Delta x_{\max}}}^{\Delta x_{\max}} |\Delta x| \cdot (2\Delta y_{\max}(\Delta x) + 1) \quad (\text{SI16})$$

due to the gauss-brackets in Δx_{\max} and more importantly $\Delta y_{\max}(\Delta x)$, we can not simplify this expression any further, but solving it numerically is very much possible. By expressing the summation limits in terms of Δy

$$\Delta y_{\max} = \left\lfloor \frac{r}{l_b} \right\rfloor \quad \Delta x_{\max}(\Delta y) = \left\lfloor \frac{r - l_b |\Delta y|}{l_a} \right\rfloor \quad (\text{SI17})$$

we find a similar expression for the value of m

$$m = \sum_{\substack{\Delta y = \\ -\Delta y_{\max}}}^{\Delta y_{\max}} |\Delta y| \cdot (2\Delta x_{\max}(\Delta y) + 1) \quad (\text{SI18})$$

Assuming a large radius compared to the lengths of the individual edges, we replace the double summation with a double integral

$$n = \sum_{\substack{\Delta x = \\ -\Delta x_{\max}}}^{\Delta x_{\max}} \sum_{\substack{\Delta y = \\ -\Delta y_{\max}(\Delta x)}}^{\Delta y_{\max}(\Delta x)} |\Delta x| \rightarrow \int_{-\frac{r}{l_a}}^{\frac{r}{l_a}} \int_{-\frac{r-l_a|x|}{l_b}}^{\frac{r-l_a|x|}{l_b}} |x| dy dx = \frac{4}{l_b(l_a)^2} \int_0^r \int_0^{r-z} z dy dz \quad (\text{SI19})$$

where the integral evaluates to

$$\int_0^r \int_0^{r-z} z dy dz = \int_0^r rz - z^2 dz = \frac{r^3}{2} - \frac{r^3}{3} = \frac{1}{6}r^3 \quad (\text{SI20})$$

such that we get

$$n = \frac{2}{3} \frac{r^3}{l_b(l_a)^2} \quad (\text{SI21})$$

and, by analogous calculations,

$$m = \frac{2}{3} \frac{r^3}{l_a(l_b)^2} \quad (\text{SI22})$$

Finally, plugging these results into equation SI11 yields main text Eq. 7:

$$\frac{n l_a^\bullet + m l_b^\bullet}{n l_a + m l_b} = \frac{\frac{2}{3} \frac{r^3}{l_b(l_a)^2} l_a^\bullet + \frac{2}{3} \frac{r^3}{l_a(l_b)^2} l_b^\bullet}{\frac{2}{3} \frac{r^3}{l_b(l_a)^2} l_a + \frac{2}{3} \frac{r^3}{l_a(l_b)^2} l_b} = \frac{l_b l_a^\bullet + l_a l_b^\bullet}{2l_a l_b} \quad (\text{SI23})$$

Supplementary Note 3: Extending the range

It is important to extend the range of 800 m to check how longer distances affect CoolWalkability. We indeed managed to triple the range from 800 m to 2400 m on the centerline networks. With up to 2400 m walk lengths, we can be confident that we cover distances that pedestrians would actually walk on a hot day, for example between their home and place of work or between touristic points of interest – if one wanted to focus on individual pedestrians. See the last columns in the new Figs. SI7-12.

The increased range has minor expected effects on CoolWalkability, such as “smoothening” the curves, as larger distances cause each starting node to reach more parts of the city, possibly traversing multiple, structurally different local neighborhoods, which causes the individual signatures of these neighborhoods to blur into each other. For example, in Manhattan (Fig. SI7) the diurnal “W” profile becomes less pronounced when extending the maximum walking distance in the centerline network (compare panel **B** with **D**) as many of the trips are now able to extend beyond the downtown area of Manhattan with high buildings and a clearly oriented grid, into neighborhoods of the city where the buildings are not as tall and the street grid is oriented differently.

The extended range covers more green areas and thus also has the natural effect of increasing differences between the scenarios that neglect and that incorporate parks, compare panels **I** and **K** in Figs. SI7-9. The biggest difference is in Manhattan (Fig. SI7) due to the inclusion of central park.

Due to our city-focused approach, where we assess CoolWalkability for each point in the city as an aggregate of potential walks from that point to all points in its local neighborhood, it is already appropriate to deal with distances that are not too long (i.e., 800 m) to quantify the *local* structures of the city. Nevertheless, the extension to 2400 m provides an important robustness check.

Supplementary Note 4: Realized routes and impacts

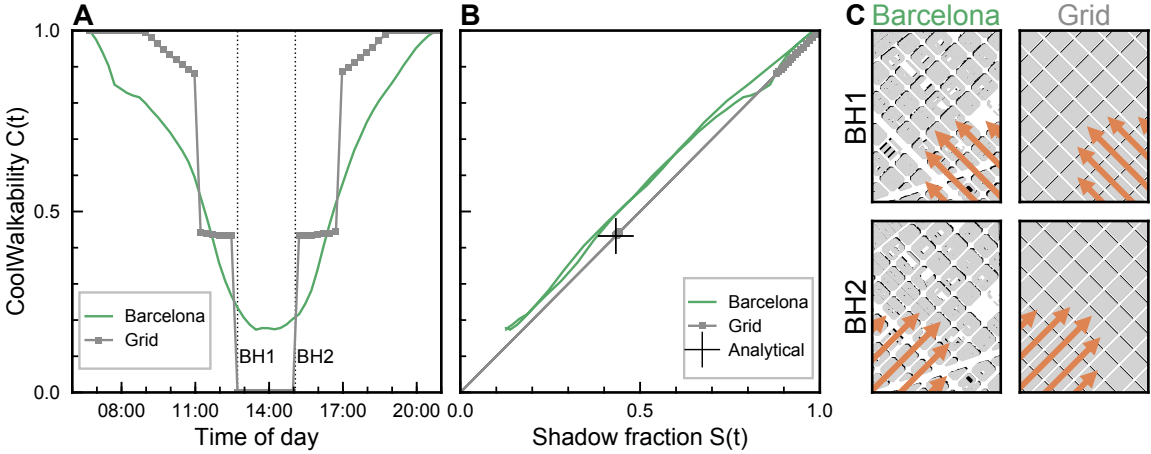
Within the context of our model, a hypothetical user would input their personal sun aversion α as the answer to the question: “How much farther are you willing to walk in the shade compared to in the sun?” Our model then finds the shortest experienced route, which is, by this definition, optimal. However, this process does not quantify how much better, if at all, the optimal route is, compared to the physically shortest route. To clarify this question, we study two simple measures.

The first measure is the relative distance traveled in the sun when using shaded routes, compared to the distance traveled in the sun when using the physically shortest paths $\frac{L^{\diamond,\alpha}}{L^{\diamond,1}}$ defined in main text Eq. 10, where $L^{\diamond,\alpha}$ is the total length traveled in the sun when optimizing for shaded routes with a sun aversion of α . The results are reported in panels E-H of Figs. SI10-12. Optimizing for shaded routes causes the relative distance in the sun during the day to decrease to values mostly between 20 % and 90 %, depending on the city, time of day, and sun aversion. For a given route, these values might help an individual decide whether it deems the proposed shaded route beneficial, compared to the shortest path. However, a small value does not necessarily imply a good performance of a given city, as the structure of the city and the available shade might limit the effect of shaded routing: For example, during noon, when there is little shade available ($S \approx 0$), the physically shortest paths are nearly the same as the experienced shortest paths, simply due to a lack of alternatives, which results in a high relative distance. To the contrary, during mornings and evenings, when the city is fully shaded ($S \approx 1$), the physically shortest paths are already efficient, and shaded routing might not affect these routes, leading again to a high value. See for example, Fig. SI10E, where $\frac{L^{\diamond,\alpha}}{L^{\diamond,1}}$ is close to 1 for low α while CoolWalkability is also close to 1. In this case, the total distances in the sun are generally fairly short, and thus even small routing changes can have strong effects, causing the resulting relative distance in the sun to fluctuate, explaining the large range of values for different α values. This becomes especially apparent at the end of the day (mornings/evenings).

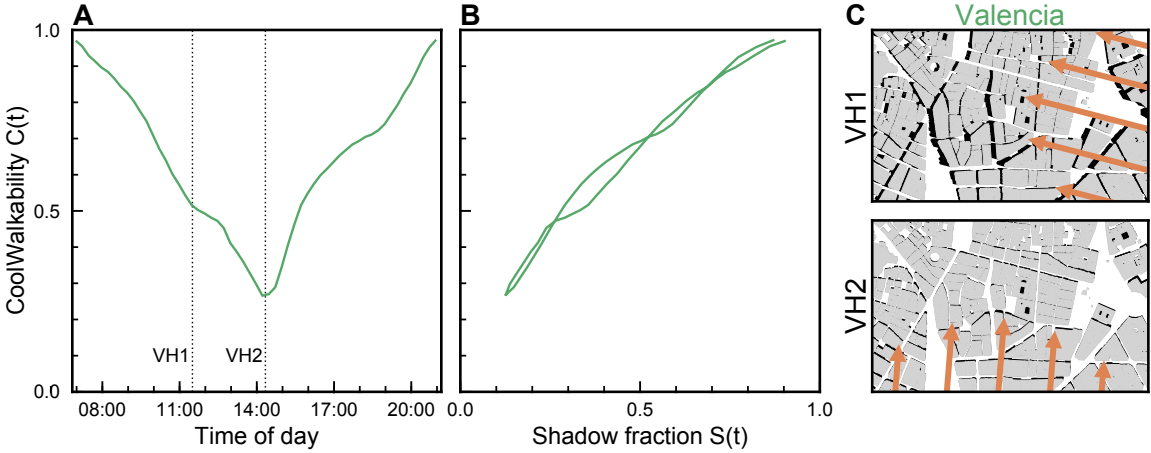
The second measure is the relative increase in physical trip-length when optimizing for shaded routes compared to the physical length of the physically shortest paths $\frac{L^{\alpha,*}}{L^{1,*}}$ defined in main text Eq. 11, where $L^{\alpha,*}$ is the total length traveled in the sun when optimizing for shaded routes with a sun aversion of α . The results are reported in panels G-I of Figs. SI10-12. The overall physical length of all paths increases only by up to 30 % at $\alpha = 10$ and stays below 10 % for values of $\alpha \leq 2$. These values are all considerably lower than the theoretically possible increase by a factor of α , as it does not happen in practice that all shortest paths are fully covered in sun while all experienced shortest paths are fully covered in shade. Concerning the concrete shapes of the daily $\frac{L^{\alpha,*}}{L^{1,*}}$ curves, it is hard to find general patterns. In general, the curves rise in the morning and fall in the evening, showing different shapes in between. Sometimes, we observe that the curves dip or fluctuate between 12:00 and 16:00. This fluctuation might be due to a “breakdown of alternatives”: as the amount of available shade decreases as the sun rises, longer and longer detours are necessary to find the shortest experienced path, especially for high α . However, at a certain point, the available shade is either not sufficient or not distributed in such a way as to facilitate shaded walks. At this point, the physically shortest paths (or some paths close to them) again become favorable, and the relative physical distance collapses. This observation, however, makes the relative distance-increase unsuitable as a measure for the performance of a city, as we do not know whether a low value is due to a favorable shade distribution or due to a general lack of options.

To understand the positive effects of reduced distance traveled in the sun, it might be beneficial to express the reduction in terms of the avoided heat-stress as well as UV exposure. While a detailed discussion of the health implications goes beyond our model, both these effects are roughly proportional to the distance walked in the sun, and as such are, in a first approximation, described by the relative distance traveled in the sun.

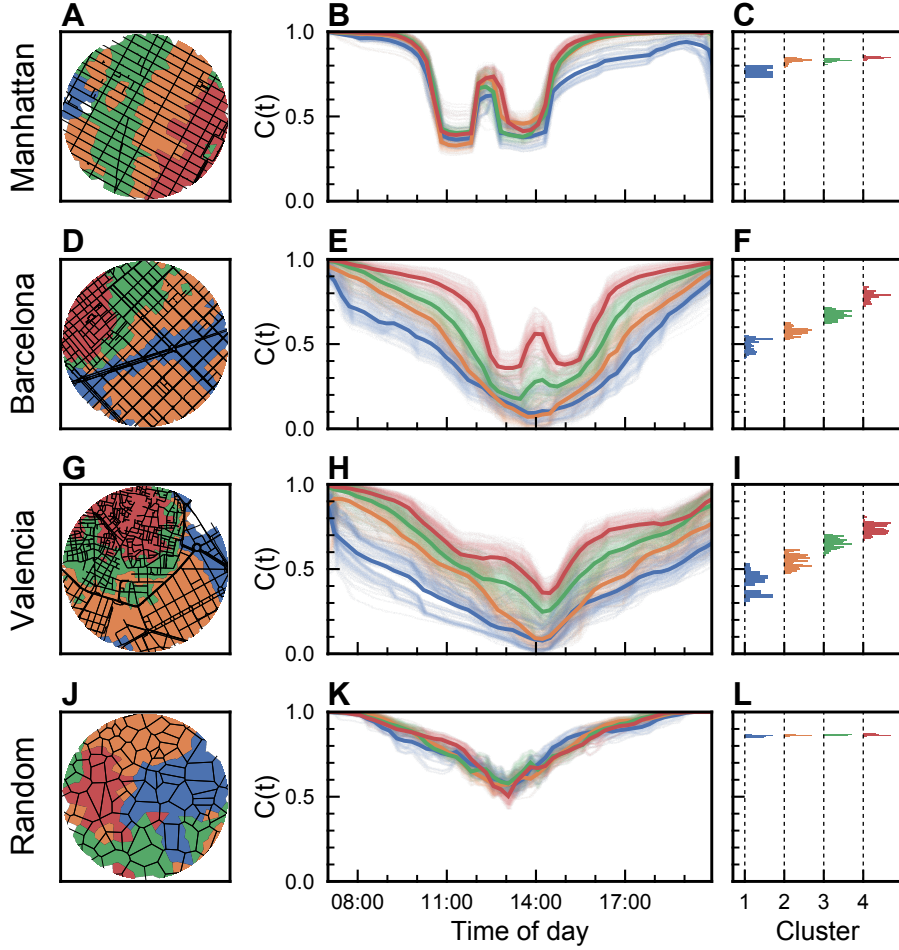
Supplementary Figures



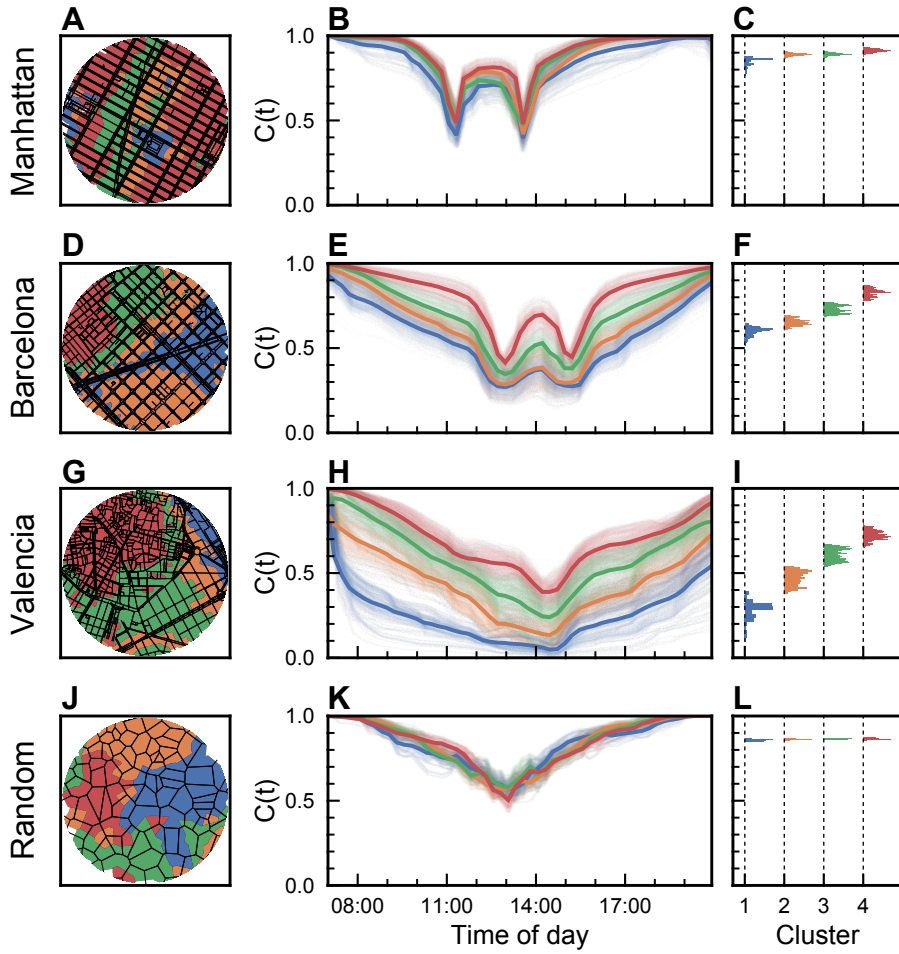
Supplementary Figure SI1: **Diurnal CoolWalkability profile and phase portrait for Barcelona.** This is a companion figure to main text Fig. 3. **A:** Due to lower, more uniform building heights, there are no noticeable “Barcelonahenge” dips (BH1 and BH2) as in Manhattan. **B:** The phase portrait shows little positive deviation of the empirical data from the grid model, implying only little CoolWalkability benefits at a given shadow fraction. **C:** Sun position showing the closest Barcelona and its grid model get to “henge” events.



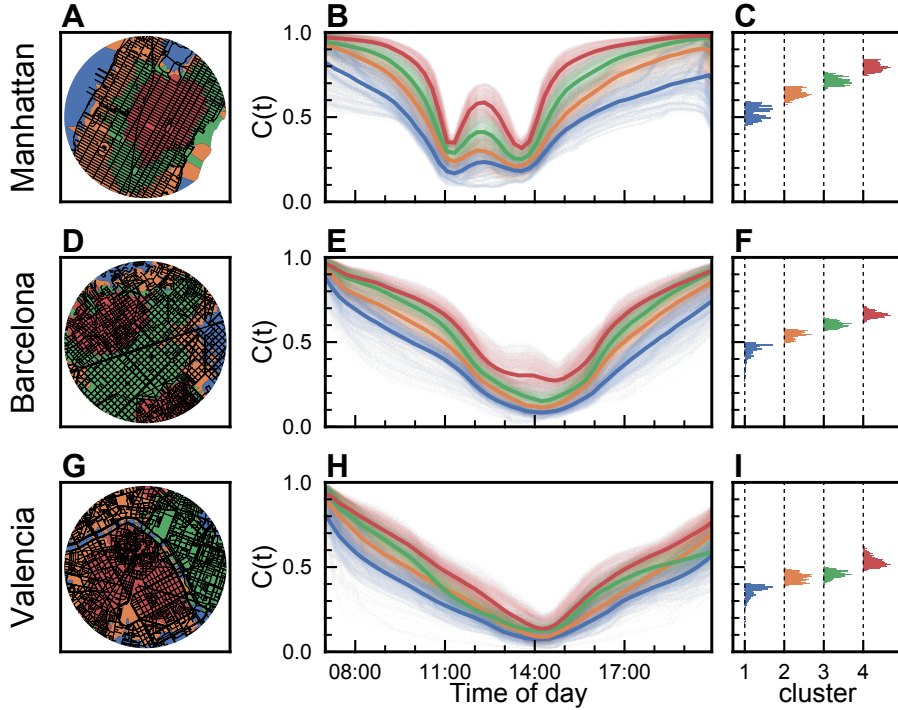
Supplementary Figure SI2: **Diurnal CoolWalkability profile and phase portrait for Valencia.** This is a companion figure to main text Fig. 3. **A:** Due to a non-grid-like street network and lower, more uniform building heights, there are no noticeable “Valenciahenge” events (VH1 and VH2) as in Manhattan. **B:** The phase portrait is similar to Barcelona, Fig. SI1, implying only little CoolWalkability benefits at a given shadow fraction. **C:** Sun position showing the closest Valencia gets to “henge” events.



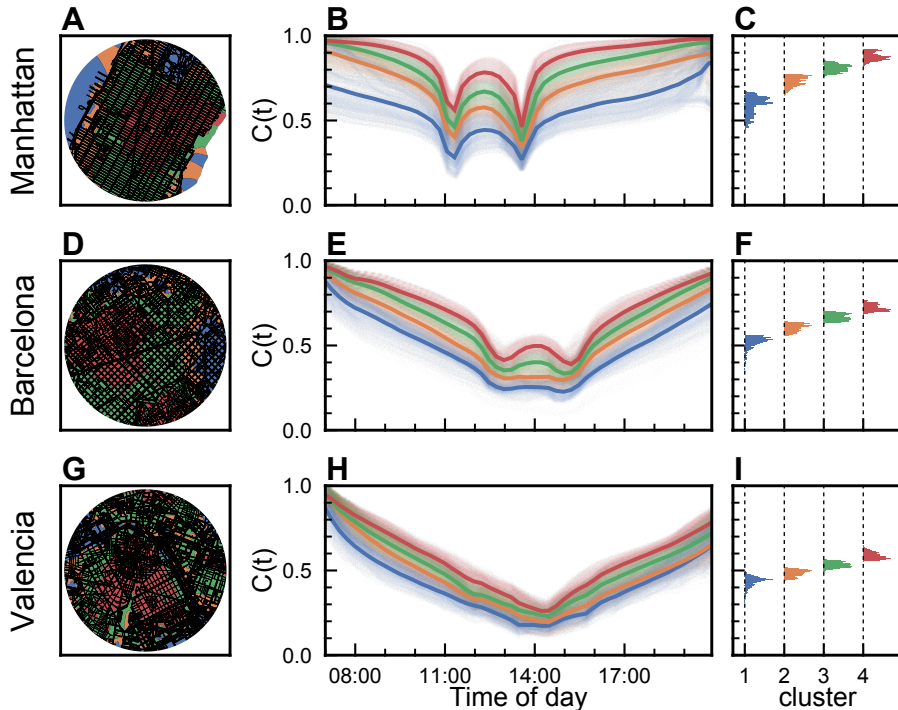
Supplementary Figure SI3: Spatial clustering by CoolWalkability leads to areas with different profiles (constant building heights). This is a companion figure to main text Fig. 5, reporting the same results but for constant building heights. From top to bottom, we study the cities Manhattan, Barcelona, Valencia, and the random null model (Poisson-Voronoi). Left column: Clustering local Coolwalkability of each node in the street network leads to spatial clusters of similar CoolWalk potential. Middle column: The diurnal profiles of these clusters display high variations within each city and between different cities. In particular, the more organic, least grid-like areas (red curves) display highest potential. **K:** The null model shows the baseline of small variation. Right column: the distributions of the time average of each diurnal profile within each cluster illustrate the large potential differences in empirical street networks. **L:** These differences are negligible in the null model.



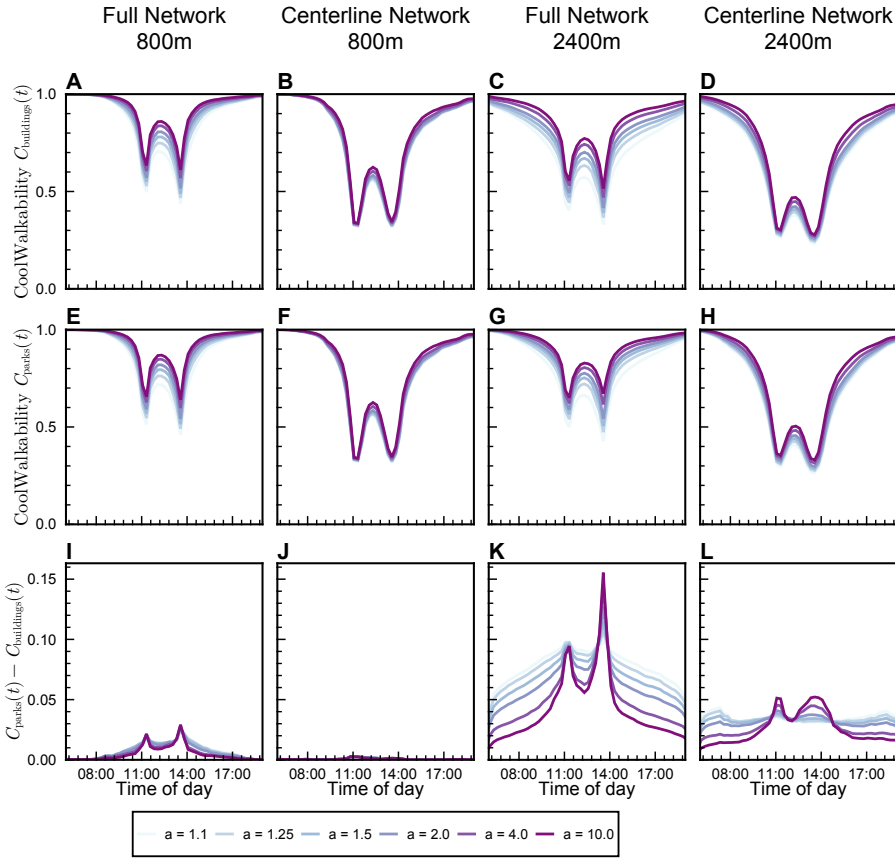
Supplementary Figure SI4: Spatial clustering by CoolWalkability leads to areas with different profiles (sidewalk network). This is a companion figure to main text Fig. 5, reporting the same results but for the sidewalk networks. From top to bottom, we study the cities Manhattan, Barcelona, Valencia, and the random null model (Poisson-Voronoi). Left column: Clustering local Coolwalkability of each node in the street network leads to spatial clusters of similar CoolWalk potential. Middle column: The diurnal profiles of these clusters display high variations within each city and between different cities. In particular, the more organic, least grid-like areas (red curves) display highest potential. **K:** The null model shows the baseline of small variation. Right column: the distributions of the time average of each diurnal profile within each cluster illustrate the large potential differences in empirical street networks. **L:** These differences are negligible in the null model.



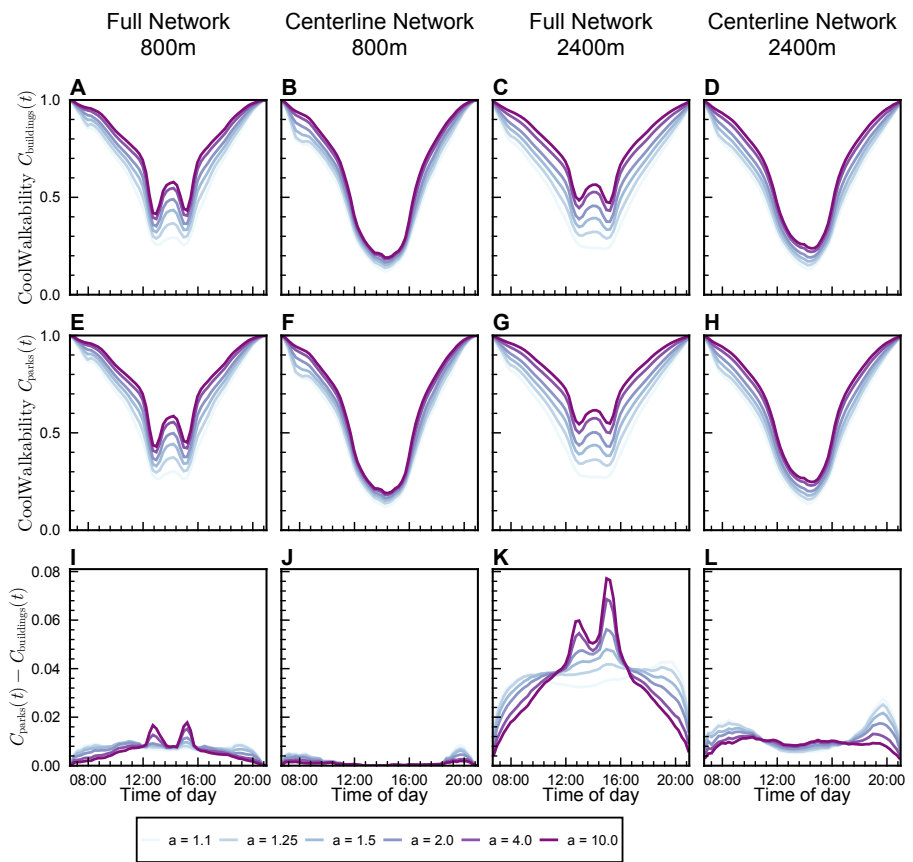
Supplementary Figure SI5: Spatial clustering by CoolWalkability leads to areas with different profiles (centerline network, 2400 m). This is a companion figure to main text Fig. 5, reporting the same results but for larger maximal walking distances. From top to bottom, we study the cities Manhattan, Barcelona and Valencia. Left column: Clustering local Coolwalkability of each node in the street network leads to spatial clusters of similar CoolWalk potential. Middle column: The diurnal profiles of these clusters display high variations within each city and between different cities. In particular, the more organic, least grid-like areas (red curves) display highest potential.



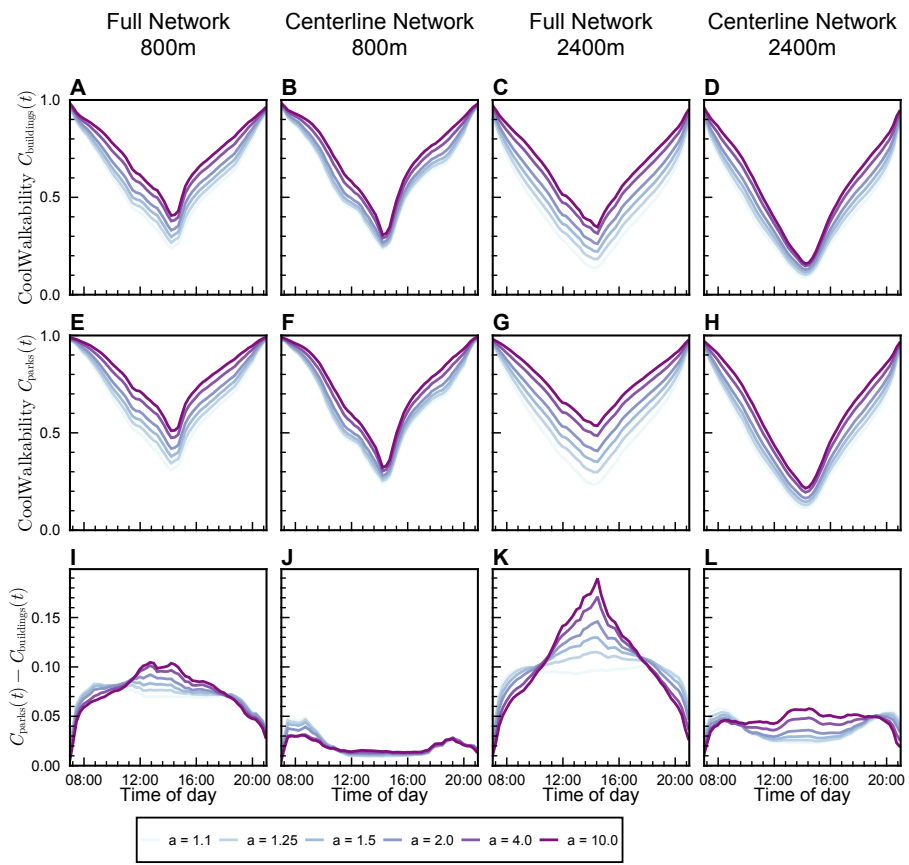
Supplementary Figure SI6: Spatial clustering by CoolWalkability leads to areas with different profiles (full network, 2400 m). This is a companion figure to main text Fig. 5, reporting the same results but for larger maximal walking distances. From top to bottom, we study the cities Manhattan, Barcelona and Valencia. Left column: Clustering local Coolwalkability of each node in the street network leads to spatial clusters of similar CoolWalk potential. Middle column: The diurnal profiles of these clusters display high variations within each city and between different cities. In particular, the more organic, least grid-like areas (red curves) display highest potential.



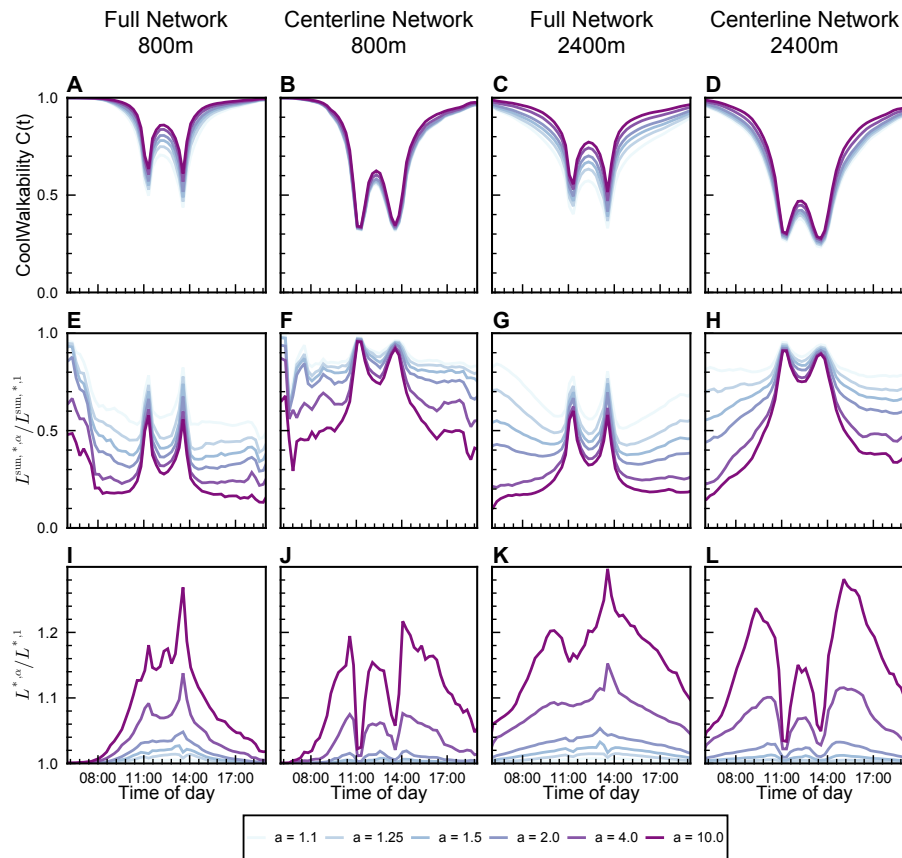
Supplementary Figure SI7: **The small effect of parks on the global CoolWalkability (Manhattan)** This figure extends the results reported in the main text by testing larger maximal trip lengths, as well as the inclusion of parks. From top to bottom, we show **A-D** the diurnal CoolWalkability-profiles for the city as defined in the main text, **E-H** for the city with the inclusion of parks, and **I-L** the difference in CoolWalkability between a city with and without parks. The difference is strongest during noon and the Manhattan-Henge events, where trees cast shade on the paths below them, while buildings provide only little shade to the paths next to them. In particular, it is strongest for the full network with extended walking distances (panel **K**), as more of the trips can be rerouted through central park.



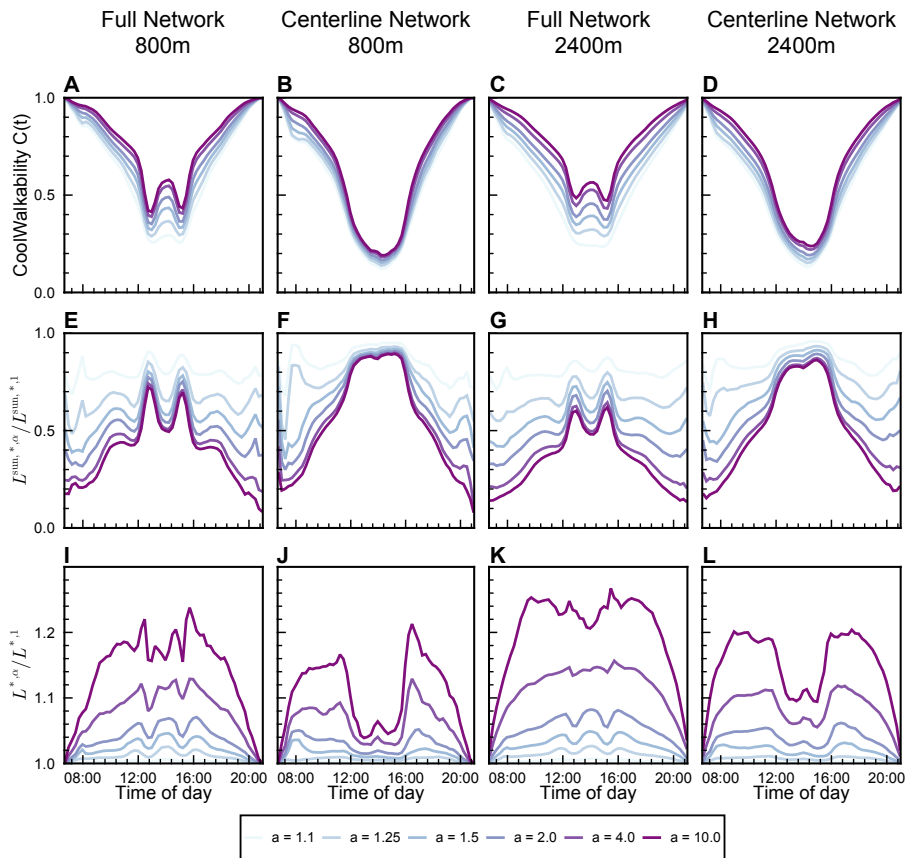
Supplementary Figure SI8: **The small effect of parks on the global CoolWalkability (Barcelona)** This figure extends the results reported in the main text by testing larger maximal trip lengths, as well as the inclusion of parks. From top to bottom, we show **A-D** the diurnal CoolWalkability-profiles for the city as defined in the main text, **E-H** for the city with the inclusion of parks, and **I-L** the difference in CoolWalkability between a city with and without parks.



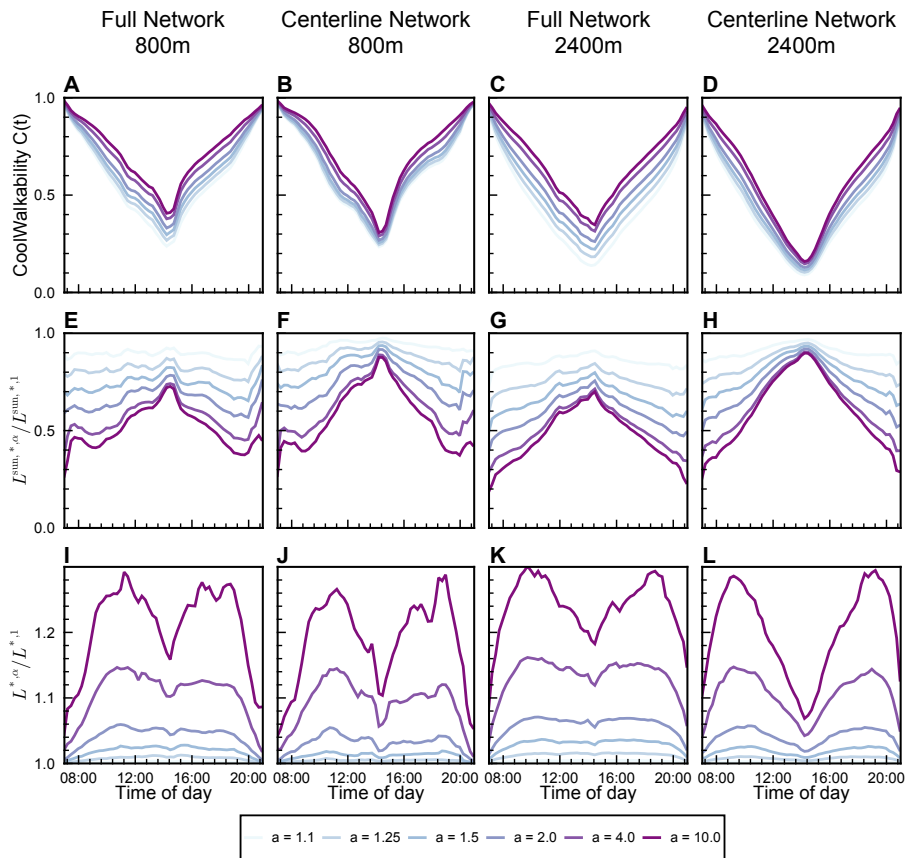
Supplementary Figure SI9: **The small effect of parks on the global CoolWalkability (Valencia)** This figure extends the results reported in the main text by testing larger maximal trip lengths, as well as the inclusion of parks. From top to bottom, we show **A-D** the diurnal CoolWalkability-profiles for the city as defined in the main text, **E-H** for the city with the inclusion of parks, and **I-L** the difference in CoolWalkability between a city with and without parks.



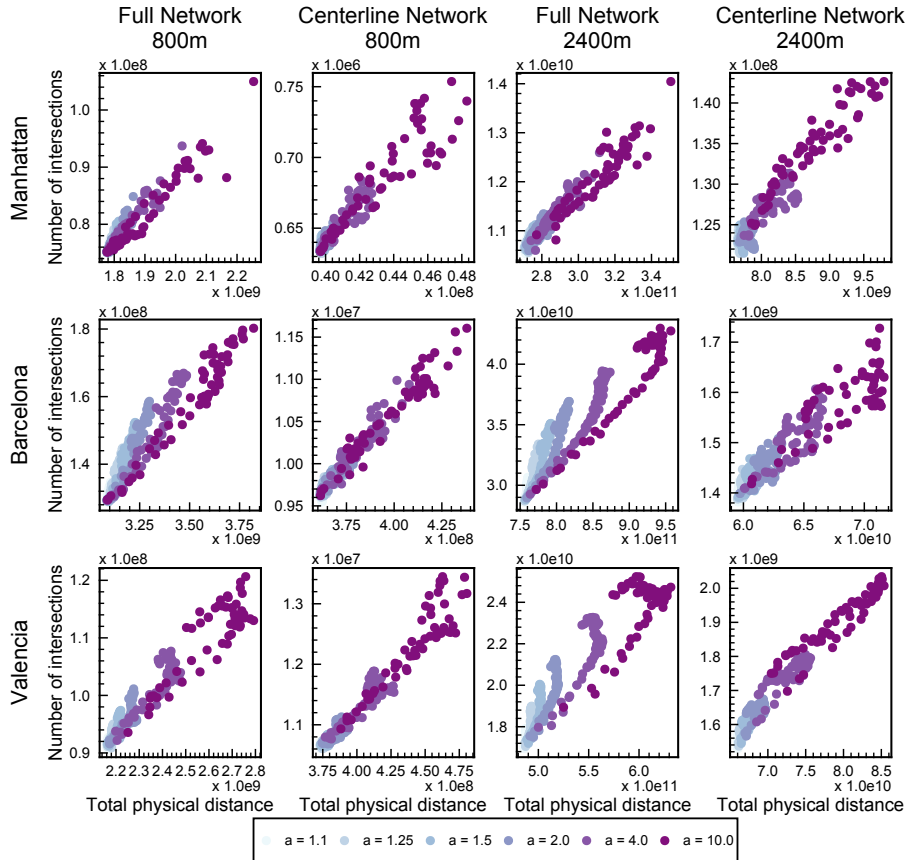
Supplementary Figure SI10: Realized impacts compared to CoolWalkability (Manhattan) This figure compares alternative measures based on the overall physical distances traveled in the sun and shade to the CoolWalkability. From top to bottom, we show **A-D** the diurnal CoolWalkability-profiles for the city as defined in the main text, **E-H** the relative distance traveled in the sun on all trips between using shaded routes (at $\alpha > 1$) and the physically shortest paths (at $\alpha = 1$) as well as **I-L** the relative total physical distance between $\alpha > 1$ and $\alpha = 1$. The relative distance in the sun generally decreases with increasing values of α , and increases, during noon.



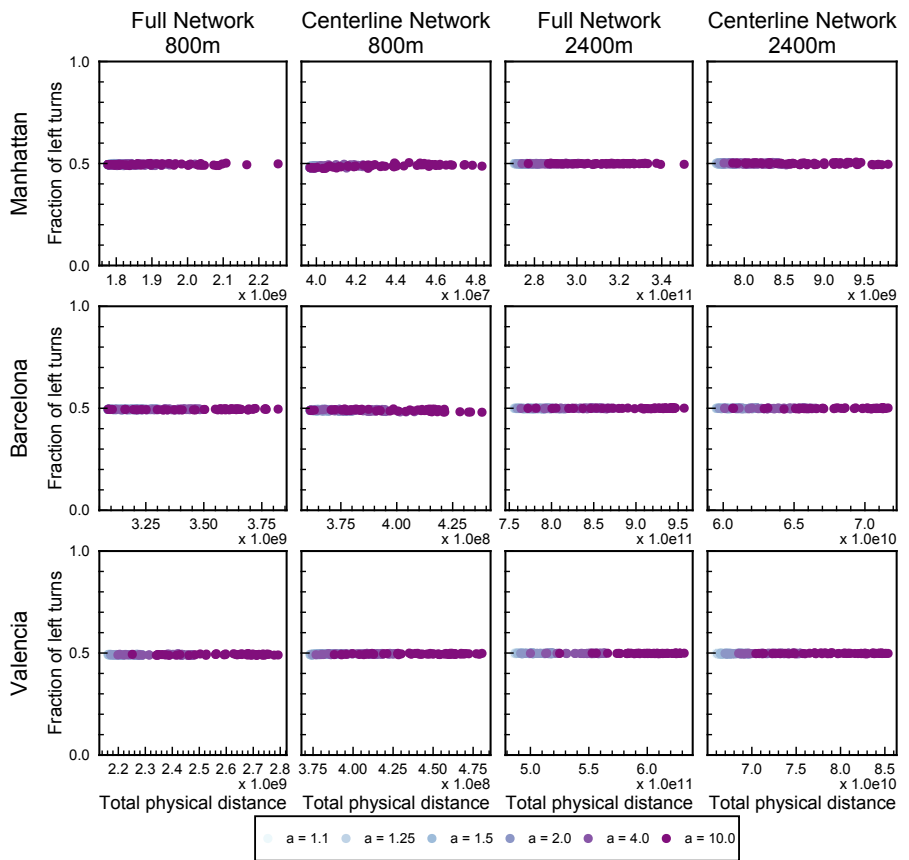
Supplementary Figure SI11: **Realized impacts compared to CoolWalkability (Barcelona)** This figure compares alternative measure based on the overall physical distances traveled in the sun and shade to the CoolWalkability. From top to bottom, we show **A-D** the diurnal CoolWalkability-profiles for the city as defined in the main text, **E-H** the relative distance traveled in the sun on all trips between using shaded routes (at $\alpha > 1$) and the physically shortest paths (at $\alpha = 1$) as well as **I-L** the relative total physical distance between $\alpha > 1$ and $\alpha = 1$. The relative distance in the sun generally decreases with increasing values of α , and increases, during noon.



Supplementary Figure SI12: **Realized impacts compared to CoolWalkability (Valencia)** This figure compares alternative measure based on the overall physical distances traveled in the sun and shade to the CoolWalkability. From top to bottom, we show **A-D** the diurnal CoolWalkability-profiles for the city as defined in the main text, **E-H** the relative distance traveled in the sun on all trips between using shaded routes (at $\alpha > 1$) and the physically shortest paths (at $\alpha = 1$) as well as **I-L** the relative total physical distance between $\alpha > 1$ and $\alpha = 1$. The relative distance in the sun generally decreases with increasing values of α , and increases, during noon.



Supplementary Figure SI13: **Number of intersections encountered compared to the total distance traveled**
 Increasing α potentially increases the total physical length of the trips traveled. With this increase in physical length, pedestrians tend to encounter more intersections, increasing the perceived complexity of a route. This figure shows that the number of intersections encountered is roughly linear in the total physical distance, showing that shade-aware routing does not increase the complexity of the experienced shortest paths beyond the complexity added due to an increased length. Only in the full network, particularly at 2400 m in Barcelona and Valencia we observe some non-linear increase for individual α values. In these particular cases it might happen that more paths can be routed through both highly shaded and intersection-dense neighborhoods of the city, thus increasing the overall number of encountered intersections beyond the linear regime.



Supplementary Figure SI14: **Fraction of left turns compared to the total distance traveled** Counting the number of turns to the left of the direction of travel and comparing this number to the full number of turns, we find no systematic bias towards either left or right turns in any of the studied cities with a change in α or the time of day.

References

- [1] Building Footprints of New York. <https://data.cityofnewyork.us/Housing-Development/Building-Footprints/nqwf-w8eh>.
- [2] Services INSPIRE of Cadastral Cartography. http://www.catastro.minhap.gob.es/webinspire/index_eng.html.